Microsecond Thermal Ablation of Skin for Transdermal Drug Delivery

Jeong Woo Lee[a], **Priya Gadiraju**[b], **Jung-Hwan Park**[c], **Mark G. Allen**[b,*], and **Mark R. Prausnitz**[a,*]

[a] School of Chemical & Biomolecular Engineering, Georgia Institute of Technology, Atlanta, GA 30332 USA

[b] School of Electrical and Computer Engineering, Georgia Institute of Technology, Atlanta, GA 30332 USA

[c] Department of BioNano Technology and Gachon BioNano Research Institute, Kyungwon University, Gyeonggi-Do, Republic of Korea 461-701

Abstract

Thermal ablation is a promising mechanism to increase permeability of the skin's outer barrier layer of stratum corneum while sparing deeper living tissues. In this study, finite element modeling predicted that the skin surface should only be heated on the microsecond timescale in order to avoid significant temperature rises in living cells and nerve endings in deeper tissue. To achieve such short thermal pulses, we developed a microdevice that rapidly heats a few microliters of water by an electrical discharge and ejects the resulting superheated steam at the skin surface on a timescale on the order of 100 μs. According to its design, we showed that this microdevice selectively removed stratum corneum of cadaver skin without significantly removing deeper tissue. This one-dimensional depth control was supplemented through the use of a masking film containing 100 μm-diameter holes placed on the skin surface during ablation to define the ablated skin area and thereby provide three-dimensional control over tissue removal. Using this approach, thermal ablation increased skin permeability to sulforhodamine B and bovine serum albumin by at least 1000-fold in vitro. We conclude that microsecond thermal ablation of skin can selectively remove stratum corneum and thereby dramatically increase skin permeability for transdermal drug delivery.

Keywords

electrical discharge; finite element model; jet; heat; skin permeability; thermal ablation; transdermal drug delivery

---

*Corresponding Authors: mallen@gatech.edu, prausnitz@gatech.edu. Send all editorial correspondence to: Mark Prausnitz, School of Chemical and Biomolecular Engineering, Georgia Institute of Technology, 311 Ferst Drive, Atlanta, GA 30332-0100 USA, Phone: +1 404 894 5135, Fax: +1 404 894 2944, prausnitz@gatech.edu.

1. Introduction

Transdermal drug delivery has a number of advantageous features, including convenient administration with a patch platform, less hepatic degradation of drugs, capability of local treatment, and rate-controlled drug delivery [1, 2]. However, conventional transdermal patches are limited to a small number of low-molecular weight, lipophilic molecules that are able to diffuse through the skin barrier, the stratum corneum, at therapeutic levels. Hydrophilic drugs and macromolecules, on the other hand, typically cannot pass through the skin at significant rates.

Transdermal administration of hydrophilic compounds and macromolecules has been explored using various technologies, including chemical, electrical, acoustic, mechanical and thermal methods. Chemical enhancers [3], iontophoresis [4] and ultrasound [5] reduce skin barrier properties by making molecular-scale rearrangements in stratum corneum lipid structures, but the stratum corneum remains largely intact, which limits the use of these approaches when delivering hydrophilic macromolecules. In contrast, mechanical and thermal approaches have been used to create micron-scale pathways across the stratum corneum, which readily permit transport of macromolecules [6]. Microneedles provide a mechanical approach that pierces across the skin to administer drugs and vaccines with high efficiency, but has the disadvantage of being invasive [7]. Thermal ablation provides a non-invasive technique to remove small portions of the stratum corneum and thereby increase skin permeability through micron-scale channels into the skin [8–13].

Transdermal drug delivery using thermal ablation is achieved by heating the skin surface to vaporize tissue, which can locally remove stratum corneum at the site(s) of heating. By keeping the thermal exposure sufficiently short, the temperature gradient across the stratum corneum can be steep enough that the skin surface is extremely hot, while the viable epidermis and deeper skin tissues do not experience a significant temperature rise. Our previous study indicated that the skin surface should achieve a temperature of hundreds of degrees Celsius, i.e., we observed only a few-fold increase in skin permeability to a hydrophilic tracer compound after heating human cadaver skin to 150 °C, but observed a 1000-fold increase after heating the skin to 300 °C [14]. In addition, modeling presented in this study predicts that heating of the skin surface should be on the microseconds scale in order to maintain a steep enough thermal gradient to protect deeper tissues.

Thermal ablation of skin has been achieved previously using a variety of methods, including arrays of microfabricated resistive [8, 9] and radiofrequency [10, 11] electrical heating elements, as well as lasers [12, 13]. The first two approaches using heating elements that contact the skin typically apply heat for on the order of 1 ms. Laser-based methods can heat the skin on the microseconds timescale, but require bulky and costly devices that are not suitable for single-use applications.

To address the limitations of previous approaches to thermal ablation, this study presents a novel microfabricated device that can rapidly convert electrical energy into thermal and mechanical energy by ejecting a jet of superheated steam at the skin on a timescale on the order of 100 μs. Capacitively discharging electric current directly through a few microliters of water in a microchamber permits extremely rapid and efficient heating of the water, which subsequently has extremely rapid and efficient heat transfer to the skin upon ejection from the device. Such a system should be sufficiently inexpensive to manufacture that it could be suitable for single-use applications as a disposable device.

The objective of this study is to (1) model heat transfer through the skin in order to determine how short the thermal exposure on the skin surface needs to be to protect viable tissue below the stratum corneum, (2) design, fabricate and validate a microdevice capable

of achieving the time-temperature profile identified through modeling and (3) assess the ability of the device to selectively remove stratum corneum and thereby increase skin permeability to hydrophilic molecules, including macromolecules. To our knowledge, this is the first study to examine thermal ablation using a jet of superheated steam applied to the skin on the microsecond timescale.

2. Materials and methods

2.1 Modeling heat penetration into the skin

The temperature profile in the skin was computed using ANSYS simulation software (ANSYS, Canonsburg, PA). We used a one-dimensional transient semi-infinite model with the boundary condition [15] that the temperature of the skin surface was held constant at 1100 °C during the thermal exposure. The duration of the thermal exposure was varied between 1 μs and 100 ms. This high temperature served as an upper estimate of the temperature of the superheated steam ejectate (see section 2.3.2). Simulations were carried out in scenarios with and without a thermally conductive mask and with and without a windows mask, as discussed below. The thermal properties of the masks [16] and the skin [17] were assumed to be constant over the entire temperature range (Table 1).

2.2 Fabrication of thermal ablation device

The thermal ablation device was designed by modifying a laminated gas generator actuator previously developed in our laboratory [18]. It has two major components: (1) a microchamber that heats and ejects superheated steam and (2) two masks that mediate the energy transfer to the skin surface.

A microchamber consisting of five patterned and integrated layers was fabricated using laser micromachining and lamination of layers. For laser micromachining, a CO_2 gas laser (LS500 Laser Engraving System, New Hermes-Gravograph, Duluth, GA) was used to cut polymer-based materials and a solid-state infrared laser (Nd:YLF, Resonetics Maestro, Nashua, NH) was used to cut metals. The microchamber was formed and bounded on four sides by cutting a rectangular hole with a nozzle exit on one side into a 250 μm-thick Mylar polymer sheet (biaxially-oriented polyethylene terephthalate (BoPET), Goodfellow, Oakdale, PA). The chamber was bounded on the remaining two sides with two brass metal electrode layers (McMaster-Carr, Elmhurst, IL). Two 1.5 mm-thick polymer backing layers (polymethylmethacrylate (PMMA), Goodfellow) were adhered to the external surfaces of the metal layers to provide structural integrity and electrical insulation of the device by adhesive lamination. This yielded a microchamber with dimensions of 1.7 mm by 2.4 mm by 250 μm and a nozzle with a height of 250 μm and a width that tapered from 150 μm at the microchamber entrance to 1500 μm at the exit.

Two different mask designs were also fabricated to facilitate mechanistic study and device optimization. The masks were placed on the surface of the skin during thermal ablation to serve as an interface between the superheated steam jet and the skin. A conductive mask was designed to efficiently conduct heat without allowing physical contact between the steam and the skin. In this case, a 25 μm-thick sheet of tungsten (3N8, ESPI Metals, Ashland, OR) was used, due to its high thermal conductivity. A "windows" mask was designed to allow heat transfer to the skin through holes (i.e., "windows") in the mask and to insulate the skin everywhere else. In this case, a 25 μm-thick sheet of titanium (3N7, ESPI Metals) was chosen due to the relatively low thermal conductivity of titanium. The titanium sheet was patterned with 100 μm-diameter circular holes in a square array with a 100 μm edge-to-edge spacing.

2.3 Characterization of the thermal ablation device

2.3.1 Measurement of voltage, current and force during device actuation—
Thermal ablation was achieved by connecting the two electrodes on either side of the microchamber to a power supply circuit. The circuit comprised a capacitor that could be charged to a certain voltage, a MOSFET switch (IRG4P254, International Rectifier, El Segundo, CA) to trigger the discharge of the capacitor through the microchamber, and two voltage measurement points (V_{high} and V_{low}) formed by resistive dividers to measure the voltage drop across the microchamber as well as the MOSFET switch. The voltage drop measured across the MOSFET was used to calculate current through the MOSFET and therefore through the microchamber according to the technical data sheet supplied by the manufacturer. The voltages were recorded using a 12-bit data acquisition board (DAQ MIO-16E, National Instruments, Austin, TX) with a junction box (BNC-2090, National Instruments).

A ring-type piezoelectric force sensor (No. 9144A21, Kistler Instruments, Amherst, NY) was attached to the microchamber to measure the ejectate reaction force generated during actuation of the device. The sensor's signal was transmitted as an electrical charge, which was amplified and recorded by the same devices used for the measurement of voltage described immediately above. During thermal ablation device actuation, in some cases a high-speed video was taken at a rate of 100,000 frames per second (EktaPro 4540, Kodak, San Diego, CA).

In some cases, the electrode surface was also analyzed by x-ray photoelectron spectroscopy (1600 XPS, Physical Electronics, Chanhassen, MN) to determine the composition of the dark material seen on the skin surface when a conductive mask was not used.

2.3.2 Estimation of superheated steam ejectate temperature—The temperature of the ejectate emitted from the microchamber was measured using an irreversible temperature-indicating film (THERMAX, Thermographic Measurements, Glenview, IL), which melts at a specific temperature when contacted with a hot object. The film was placed under a conductive mask to avoid mechanical damage to the film from direct contact with the steam ejectate, and the temperature of the heat transferred through the conductive mask was measured. The detectable temperature ranged from 30 °C to 290 °C.

The ejectate temperature was also estimated theoretically. To provide an upper estimate of temperature, we assumed that all electrical energy applied to the microchamber was used to heat and boil the water in the chamber, as described in the following equation,

$$E=(mC_{p,liq}\Delta T_{liq})_{water}+m\Delta H_{vap}+(m\int C_{p,vap}dT)_{steam} \tag{1}$$

where E is the total amount of electrical energy consumed (4.6 J), m is the mass of water in the microchamber (1 mg), ΔT_{liq} is the temperature change from room temperature (25 °C) to the normal boiling point (100 °C), $C_{p,liq}$ is the specific heat of liquid water (4.186 J/g·°C), ΔH_{vap} is the specific heat of vaporization at the normal boiling point (2255 J/g) and $C_{p,vap}$ is the specific heat of steam ($C_p(T) =(33.46 + 0.688\times10^{-2}\,T + 0.7604\times10^{-5}\,T^2 - 3.593\times10^{-9}\,T^3)/18.016$ J/g·°C) integrated from 100 °C to the final temperature [19].

2.4 Thermal ablation of skin in vitro

2.4.1 Thermal ablation of skin—First, 1 μl of phosphate buffered saline (PBS) was filled into a microchamber, the chamber was attached to the piezoelectric force sensor, and the two electrodes in the microchamber were connected to the power supply circuit. Then, a

piece of full-thickness pig cadaver skin was trimmed to fit the size of the nozzle exit hole from the microchamber and pushed slightly into the nozzle exit hole using a cotton swab to hold the skin in place. In some cases, as described immediately below, a mask was placed on the surface of the skin before positioning it at the nozzle exit hole. The pig skin was prepared with IACUC approval by removing the subcutaneous fat with a scalpel and the hair with a shaver (Series 8900, WHAL, Sterling, IL).

As described in Table 2, the skin was ablated according to one of four different scenarios using different mask arrangements. In Group 1, no mask was employed, which allowed the superheated steam ejectate to directly contact the skin. In Group 2, a windows mask was used so that the steam ejectate only contacted the skin through the holes in the mask. The parts of the skin covered by the mask were insulated by the mask. In Group 3, a conductive mask was used, so that the heat of the steam ejectate could be efficiently transferred to the skin, but any mechanical or chemical component of the steam-skin interaction would be blocked. Finally, in Group 4, both a conductive mask and a windows mask were placed on the skin. In this way, only the skin exposed through the windows were heated by the steam ejectate.

2.4.2 Imaging of skin after thermal ablation—Before and after thermal ablation treatment, pig skin samples were viewed by brightfield microcopy (SZX12, Olympus). In some cases, a hydrophilic model drug, sulforhodamine, was applied to the skin surface for 30 min or 12 h (unless otherwise indicated) and then removed before imaging. The formulation consisted of 1 ml of deionized water containing 30 mg/ml sulforhodamine B (Molecular Probes, Eugene, OR) and 100 mg/ml carboxymethylcellulose (Cat No. 360384, Aldrich, Milwaukee, WI). After brightfield observation, each skin sample was prepared for histology. Skin samples were frozen in histology mounting compound (Tissue-Tek, Sakura Finetek, Torrance, CA) and sliced into 20 μm-thick sections (Cryo-star HM 560MV, Microm, Waldorf, Germany), which were mounted and viewed by brightfield and fluorescence microscopy (E600, Nikon, Tokyo, Japan).

2.5 Skin permeability measurement

Human cadaver skin was obtained with approval from the Georgia Tech Institutional Review Board and either left intact or exposed to thermal ablation over an area of 3 mm^2. When a windows mask was used, this treated area exposed 20 holes in the mask. The skin was then placed between the donor and receptor compartments of a Franz diffusion cell (Permegear, Hellertown, PA). The donor compartment was filled with either 10^{-3} M sulforhodamine B (558 Da, Molecular Probes) or 10^{-4} M Texas Red-labeled bovine serum albumin (BSA, 66,000 Da, Molecular Probes) in PBS, and the receptor compartment was replenished with fresh PBS after each sampling. Measurements of drug concentration were taken periodically for up to 48 h using spectrofluorimetry (QM-1, Photon Technology International, South Brunswick, NJ). At the end of the experiment, the skin was prepared for histological analysis, as described above.

3. Results and Discussion

The goal of this study is to develop a skin ablation method that selectively removes the stratum corneum skin barrier without damaging viable epidermis or dermis in order to minimize tissue trauma and pain. To achieve this goal, a critical question is how long the ablation energy should be applied to the skin surface to effectively ablate stratum corneum without generating a significant temperature change in deeper tissue.

3.1 Modeling heat transfer into skin

To guide device design and operation, we first carried out finite element modeling of the temperature profiles generated in skin after thermal ablation under a number of different conditions. Our goal was to identify the longest thermal exposure that does not allow significant heat to reach the viable epidermis. In experimental studies described below, we considered four different scenarios in which the skin was covered in different ways using masks (see Table 2). In these four different scenarios, heat could be transferred to the skin by the superheated steam ejectate from the thermal ablation device in one of three ways, which are summarized in Fig. 1A.

In Case I, the superheated steam directly contacts the skin. In Case II, there is a thin film of highly conductive metal (i.e., conductive mask) through which heat is transferred from the steam ejectate to the skin, which may be exposed through the open holes in a windows mask. In Case III, there is both a conductive mask and the insulating portion of a windows mask through which heat is transferred. The conductive mask is designed to efficiently transfer heat, whereas the insulating portion of the windows mask is designed not to conduct heat well.

In Case I, when the skin is directly exposed to superheated steam at 1100 °C, which is the highest estimated output of our thermal ablation device, there is a strong dependence on the thermal exposure time. As shown in Fig. 1B, the viable epidermis has no significant temperature rise after exposures of 1 μs, 10 μs and 100 μs. Because heat transfer is slowest in the stratum corneum layer, which has the lowest thermal conductivity of all the skin layers, heat barely penetrates into the viable epidermis during these short exposures. After a 1 ms exposure, the viable epidermis is heated to a temperature of 180 °C, and becomes still hotter after longer exposures. These temperatures are well above those expected to injure cells [20] and cause pain (42 °C) [21], and therefore should be avoided.

Fig. 1E shows the calculated temperatures at the stratum corneum – viable epidermis interface and the epidermis – dermis interface as a function of thermal exposure time. This graph re-enforces the point that thermal exposures on the order of 100 μs or less are expected to avoid heating viable epidermis, whereas exposures on the order of 1 ms or more are not. Model simulations further predict that heat penetration all the way to the dermis takes an order of magnitude longer, such that thermal exposures on the order of 1 ms or less avoid heating dermis, whereas exposures on the order of 10 ms or more penetrate to the dermis.

It may sometimes be desirable to avoid direct contact between the superheated steam ejectate and the skin, which can be achieved using a conductive mask, as in Case II. As shown in Fig. 1C, the mask design used in this study permits sufficient heat transfer that the skin surface temperature is almost the same as the ejectate temperature after millisecond exposures, but is significantly lower after microsecond exposures. After a 100 μs thermal pulse, the skin temperature is 920 °C, which is 16 % lower than the ejectate temperature. These data suggest that heating the skin for on the order of 100 μs may be optimal when using this conductive mask because that exposure time is long enough to allow the skin surface to be substantially heated, but still short enough to avoid heating below the stratum corneum. Different conductive mask designs, for example involving different mask materials or thickness, would lead to different characteristic times for heat penetration across the mask.

Finally, in some cases it may be desirable to use a windows mask that allows skin heating through the holes in the mask, but protects the skin that is covered by the insulating regions of the mask, as in Case III. Fig. 1D shows that the insulating regions of the windows mask

used in this study provide effective insulation for thermal exposures on the order of 10 μs or less, partial insulation at 100 μs, and little or no effective insulation at 1 ms or longer. Better insulation could be achieved if the windows mask had been made of a different material, such as a thin polymer film [16].

Our simulations emphasized thermal ablation at 1100 °C. However, ablation may be carried out at lower temperatures too. As shown in Fig. 1F, the characteristic time to increase the temperature of the stratum corneum – viable epidermis junction by 10 °C is relatively insensitive to skin surface temperature over the range of temperatures considered from 100 °C to 1100 °C, and remains at or somewhat below 1 ms. Likewise, the characteristic time to heat the epidermis –dermis junction by 10 °C is on the order of 10 ms over this temperature range. Although tissue removal localized to the stratum corneum barrier layer minimizes tissue damage, it may sometimes be acceptable, or desirable, to also remove viable epidermis too. Because sensory neurons reside mostly near the epidermal – dermal junction [22], heat penetration into the viable epidermis, but not the dermis, could avoid pain and still be achieved with millisecond thermal exposures.

3.2 Design and fabrication of thermal ablation device

Guided by the heat transfer simulation results, we designed a thermal ablation device to achieve thermal exposures on the order of 100 μs. Previous approaches to heating skin have used electrical heating elements, which can be inexpensively manufactured, but typically heat skin on the milliseconds timescale [8–11], or lasers, which can heat the skin on the microseconds timescale, but require costly instrumentation that is not suitable for single-use applications [12, 13]. The approach developed in this study is designed to achieve thermal ablation on the 100 μs timescale using a low-cost, disposable device suitable for mass production.

To transfer energy on such a rapid timescale, we decided to pass current directly through saline by an electrical discharge that vaporizes the water and ejects the resulting superheated steam onto the skin's surface. This approach lends itself to inexpensive mass production, because the power requirements are relatively small (e.g., similar to those needed to activate the flash on a disposable camera) [23] and the device can be fabricated from inexpensive materials using a simple manufacturing process.

Our thermal ablation device contains a microchamber (Fig. 2A), in which an electrical discharge is used to heat and vaporize water, and a power circuit (Fig. 2B) to supply electrical energy to the microchamber. The microchamber was batch fabricated by laser micromachining five polymer or metal sheets and then laminating them together. As shown in Fig. 2A, the chamber, including an exit nozzle through which the steam ejectate is discharged, is defined by a central polymer sheet. The upper and lower surfaces of the chamber are made of metal sheets that serve as the electrodes. Finally, two outer backing layers are included to provide mechanical strength and electrical isolation of the device.

One batch containing 16 devices, each with two microchambers, is shown in Fig. 2C. Each device is circular with a 1.8 cm radius. The dark-colored microchambers are located at the 1 o'clock and 7 o'clock positions on each device. In these prototype devices, the nozzles point radially outward so that the ejectate is emitted from the outer edge of the device. Future designs could adjust the geometry to eject the steam jet from the upper or lower face of the devices (i.e., out of the plane of the image shown in Fig. 2C), which may be better integrated into a patch-like format. In addition, more microchambers could be fabricated in each device, or, alternatively, device size could be reduced to accommodate only one microchamber each.

The electrodes of the microchamber are connected to a power supply circuit (Fig. 2B), in which a capactive discharge drives current through the microchamber. The electrical energy stored in the capacitor is discharged rapidly with the MOSFET switch on, generating an electrical discharge between the two electrodes in the microchamber. This nearly instantaneous event heats, vaporizes and ejects the saline from the microchamber through the nozzle, indicating the rapid transformation of electrical energy into thermal and mechanical energy that can be used for skin ablation. The thermal ablation device is shown in Fig. 2D mounted with the force sensor used to measure the force of the steam jet being ejected, and the electrical connections to the power supply. Fig. 2E shows a single frame from a high-speed video taken during thermal ablation device activation, which captures the steam jet being ejected from the nozzle.

3.3 Characterization of thermal ablation device

3.3.1 Timescale of steam jet ejection—We next tested the design criterion that the thermal ablation device operates on a timescale on the order of 100 μs. The video image shown in Fig. 2E gives a first assessment of this timescale. Because the video operated at a rate of 100,000 frames per second (i.e., 10 μs per frame) and the ejectate was only seen in one frame, this indicates that the steam jet was ejected within 10 μs at the most.

As a more precise measure of ejection kinetics, we measured the voltage and current in the microchamber. As shown in Fig. 3A, the voltage across the microchamber rapidly rises and peaks at 6.7 μs, which is followed by a sudden voltage drop until approximately 53.3 μs (i.e., the inflection point in the voltage curve in Fig. 3A). This is where the primary electrical discharge occurs. Then, there is a steady decay in voltage until 1.3 ms, at which point the MOSFET switch turns off. During this time, the current saturates for the first 193 μs and then decays until 1.3 ms (Fig. 3A)

Force measurements were also made during device actuation. As shown in Fig. 3B, the force exerted during electrical discharge in the microchamber peaks at 100 μs, which corresponds to the timescale over which the primary steam ejection occurs. The force curve then oscillates and decays, which is due to resonance of the apparatus and dissipation of the reaction force energy, but is not believed to reflect forces generated directly by the steam jet ejection.

Altogether, these data suggest that steam is generated and ejected from the microchamber on a timescale on the order of 100 μs, while continued heating that does not appear to be associated with primary jet formation occurs until 1.3 ms, after which the switch is turned off.

3.3.2 Temperature of energy medium—Next, we measured and calculated the temperature of the hot steam ejected from the microchamber. In an attempt to directly measure the ejectate temperature, we placed temperature-indicating films with a detection range of 30 °C to 290 °C at the microdevice nozzle exit during activation. The ejectate temperature exceeded the range of the films, indicating that the steam jet exceeded a temperature of 290 °C. More precise experimental measurement of temperature was not possible with the equipment available to us.

We also used the data in Fig. 3A in combination with Eq. 1 to calculate the maximum temperature of the ejectate. As shown in Fig. 3A, the total energy consumed by the electrical discharge was 4.6 J. The substitution of that value into the energy balance shown in Eq. 1 yields a temperature of 1035 °C. This is an upper estimate of temperature, because it assumes that all electrical energy is transferred to the water with no losses to the surroundings. Bounded by the measured lower limit and the calculated upper limit, we

conclude that the temperature of the steam ejectate was between 290 °C and 1035 °C. In the calculations reported above, we used 1100 °C as the maximum ejectate temperature as a conservative, upper-bound value, although we expect the actual temperature was probably lower.

3.4 Thermal ablation of skin

3.4.2 Ablation of pig cadaver skin—The microsecond thermal ablation device was activated with pig cadaver skin positioned at the nozzle exit to ablate the skin. As shown in Fig. 4A, the left side of the skin, which was not exposed to the steam ejectate, contains the three characteristic skin layers: the upper, non-stained layer of stratum corneum, the blue-stained viable epidermis and the red-stained dermis. The right side of the skin was exposed to thermal ablation without the use of a mask (i.e., Group 1 in Table 2). The red-stained dermis and the blue-stained viable epidermis are still present, but the stratum corneum has been selectively removed. The continuous staining of the viable epidermis indicates that the skin indentation at the site of ablation was formed by the ablation device as a skin surface deformation, not by tissue removal or damage.

In order to reduce the area of tissue removal, a windows mask was placed over the skin to localize ablation of the stratum corneum. This mask had holes of 100 μm diameter, which roughly corresponds to the areas of tissue removal shown in Fig. 4B. With the use of the mask, tissue removal was controlled in three dimensions, where the thermal ablation operating parameters controlled depth of tissue removal and the mask controlled the area.

Closer examination of the images in Fig. 4 shows evidence of black material at the sites of ablation. These black deposits were also seen on the electrode surface in the microchamber (data not shown). Because it was difficult to directly analyze the skin, we analyzed the black debris on the electrode surface by X-ray photoelectron spectroscopy (XPS). The XPS data suggested that the deposited material is probably a mixture of melted polymer and the metal electrode. We believe this byproduct of the electrical discharge is also the source of black material on the skin surface (i.e., the black material on the skin surface is not burned skin). This point is further addressed below in the context of the conductive mask.

3.4.3 Skin ablation with conductive and windows masks—Guided by the hypothesis that the black material on the skin surface is a byproduct of the electrical discharge that is carried to the skin by the steam ejectate, we placed a conductive mask over the skin surface. This mask provided a physical barrier that prevented the steam ejectate and any entrained particles from contacting the skin. This mask also provided a thermally conductive pathway to transfer heat from the steam ejectate to the skin surface. In this way, the conductive mask allowed the thermal ablation device to heat the skin without exposing the skin to debris ejected from the device.

Fig. 5 shows an untreated, negative control skin before (Fig. 5A) and after (Fig. 5B) exposure to pink-colored sulforhodamine for 12 h without skin ablation. Although the hairs were stained, the skin surface was not stained, indicating that it was intact. Figs. 5C and 5D show skin treated with skin ablation using the conductive mask. After ablation, but before applying sulforhodamine, the skin surface is indistinguishable from the negative control skin (Fig. 5C). There is no visible evidence of skin damage at this level of magnification, and there is no evidence of the black debris seen previously without the conductive mask. After applying sulforhodamine to the ablated skin (Fig. 5D), the skin surface was heavily stained, which indicates a breach in the stratum corneum barrier at the site of ablation.

Histological images of skin ablated with a conductive mask are shown in Fig. 6. The untreated, negative control skin shows no penetration of dye when viewed under brightfield

(Fig. 6A) or fluorescence (Fig. 6C) imaging. H&E-stained skin appeared intact (Fig. 6E). In contrast, thermally ablated skin showed penetration of sulforhodamine into the skin (Figs. 6B and 6D) and selective removal of stratum corneum (Figs. 6B and 6F). The intense coloring at the surface of the skin shown in Fig. 6B appears to be dark pink staining from sulforhodamine, in contrast to the black debris seen before in Fig. 4B. The skin shown in Fig. 6F similarly lacks the black staining seen when the thermal ablation was carried out without the conductive mask.

The use of the conductive mask can also provide mechanistic insight. This mask not only keeps debris away from the skin, but also blocks mechanical effects of the steam ejectate on the skin. Without the conductive mask, the steam jet not only transfers thermal energy to the skin, but also has a mechanical impact due to its high velocity. The fact that the skin was ablated both with and without the conductive mask suggests that the thermal effect is the dominant mechanism by which the steam ejectate affected the skin.

An optimal design could involve the use of both the conductive mask, to keep debris away from the skin, and the windows mask, to control the ablated skin area. We therefore ablated the skin using both a conductive mask and windows mask to cause localized removal of the stratum corneum. Brightfield imaging of the skin surface appeared similar to untreated skin (Fig. 7A), but the localized ablation sites were evident after 30 min exposure to sulforhodamine, as shown in Fig. 7B. We confirmed the localized and selective removal of stratum corneum by histological imaging using brightfield (Fig. 7C) and fluorescence optics (Fig. 7D).

3.5 Skin permeability measurements

Selective removal of stratum corneum is expected to increase skin permeability. We therefore measured rates of transdermal transport across full-thickness human cadaver skin for two hydrophilic, fluorescent model compounds: sulforhodamine and Texas Red-labeled BSA. As shown in Fig. 8, intact skin that was not treated with thermal ablation did not have significant levels of transdermal delivery of sulforhodamine or BSA over the 24 – 48 h study period (i.e., the permeability of intact skin for both molecules was below the detection limit of 3×10^{-6} cm/h). This observation was confirmed through histological imaging, which also showed essentially no penetration of these model compounds into the skin (Fig. 9).

In contrast, thermally ablated skin showed a remarkable increase in the transdermal flux of both molecules. After a lag time of 6.0 ± 2.0 h, skin permeability to sulforhodamine was $3.1 (\pm 0.9) \times 10^{-2}$ cm/h. After a lag time of 11.7 ± 4.8 h, skin permeability to BSA was $3.6 (\pm 0.8) \times 10^{-3}$ cm/h. This corresponds to at least a 10^4-fold increase in permeability to sulforhodamine and a 10^3-fold increase in permeability to BSA after thermal ablation compared to intact, untreated skin (Fig. 8). Note that this study used full-thickness human cadaver skin, which provides a significantly greater diffusional barrier compared to drug delivery in vivo, for which a drug needs only to penetrate to the capillary bed in the superficial dermis for systemic delivery. For this reason, permeability could be an order of magnitude larger and lag time could be an order of magnitude shorter in vivo. Histological imaging similarly showed significant penetration of both compounds deep into the skin after ablation (Fig. 9).

4. Discussion

The goal of this study was to design a method for applying energy quickly to the skin that enables three-dimensional control over the selective removal of stratum corneum without causing damage to deeper skin tissue. To achieve this goal, we developed a microsecond thermal ablation system to create a rapid energy transfer to the skin surface based on an

electrical discharge and an ejected jet of superheated steam. The duration and temperature of the steam ejectate was used to control the depth of tissue removal (depth control) and the use of a windows mask localized tissue removal to micron-scale spots on the skin surface (lateral control). The further use of a conductive mask prevented physical contact between the ejectate and the skin surface, which thereby prevented black particles entrained in the steam jet from contacting and discoloring the skin. While skin ablation of spots measuring approximately 100 μm in diameter were achieved in this study through the thickness of the stratum corneum, the use of different mask sizes and different ablation operating parameters could achieve different degrees of tissue removal, if desired.

Previous studies have also investigated thermal ablation as a mechanism to increase skin permeability. Laser-based approaches have achieved controlled skin tissue ablation using microsecond pulses [12, 24], but require instrumentation that is currently sold for thousands of U.S. dollars (e.g., Epiture EasyTouch™ (Norwood Abbey, Bayside, Victoria, Australia) was sold for approximately $5,000 [25]. Devices are also under development for thermal ablation using resistive and radiofrequency heating that employ non-disposable power supplies coupled to disposable heating elements. These devices apply heat for on the order of 1 ms and generate holes in the skin that have been reported to penetrate beyond the stratum corneum and into the viable epidermis and dermis [10, 26].

In comparison with other technologies under development, we believe the thermal ablation device presented in this study can achieve optimal tissue removal using a simple, inexpensive, single-use device. We define optimal tissue removal as (i) selective removal of the stratum corneum barrier without damaging deeper tissue to minimize tissue damage and (ii) ablated spots of micron-scale dimensions (e.g., 100 μm diameter) to avoid undesirable cosmetic appearance and enable rapid healing. We believe the device design developed in this study can be inexpensive during mass production because the device itself is produced simply by cutting and laminating sheets of metal and polymer and the power supply has requirements similar to those of the flashbulb in a disposable camera [23]. We therefore believe the complete thermal ablation system could be mass produced at a cost well that enables disposable use in many healthcare markets.

Mechanistically, the thermal ablation device developed in this study can have both a thermal and mechanical interaction with the skin, which differs from previous devices in the literature. However, through the use of the conductive mask, which blocks mechanical interaction of the jet with the skin, we showed that the thermal component of the steam ejectate was the dominant mechanism of skin ablation in this study.

Finally, it is significant to note that skin permeability was increased not only to a low molecular weight, hydrophilic molecule (sulforhodamine), but also to a large protein macromolecule (BSA). Given the 100-μm diameter of the pores created using the windows mask, it appears that drugs of almost any molecular weight should be able to enter the skin. High molecular weight drugs may, however, still enter the skin less efficiently because of the inherently slower rate of diffusion through the pores due to the inverse relationship between molecular weight and diffusion coefficient [27].

5. Conclusion

Through modeling, we determined that thermal ablation should occur on the 100 μs time scale in order to ablate the stratum corneum without damaging deeper tissues. To generate the high temperatures needed for skin ablation on this time scale, we designed a microdevice that rapidly heats water by an electrical discharge, thereby ejecting a superheated steam jet at the skin surface. We found that this device was able to selectively ablate stratum corneum

and, when combined with a windows mask, enabled three-dimensional control over tissue removal. The use of a conductive mask isolated the skin from physical contact with the steam jet and any entrained particles or debris. This system was shown to increase skin permeability to sulforhodamine and BSA by at least 10^4-fold and 10^3-fold, respectively. Overall, this study introduces the first thermal ablation device based on microsecond ejection of a jet of superheated steam. This technology may enable transdermal delivery of a wide variety of hydrophilic drugs and macromolecules using a low-cost, fully disposable device.

Acknowledgments

References

1. Prausnitz MR, Langer R. Transdermal drug delivery. Nat Biotech. 2008; 26(11):1261–1268.

2. Bronaugh, RL.; Maibach, HI. Percutaneous absorption: drugs, cosmetics, mechanisms, methodology. Taylor & Francis; Boca Raton: 2005.

3. Williams AC, Barry BW. Penetration enhancers. Adv Drug Deliver Rev. 2004; 56(5):603–618.

4. Subramony JA, Sharma A, Phipps JB. Microprocessor controlled transdermal drug delivery. Int J Pharma. 2006; 317(1):1–6.

5. Ogura M, Pahwal S, Mitragotri S. Low-frequency sonophoresis: Current status and future prospects. Adv Drug Deliver Rev. 2008; 60(10):1218–1223.

6. Arora A, Prausnitz MR, Mitragotri S. Micro-scale devices for transdermal drug delivery. Int J Pharma. 2008; 364(2):227–236.

7. Prausnitz MR, Mikszta JA, Cormier M, Andrianov AK. Microneedle-based vaccines. Curr Top Microbiol Immunol. 2009; 333:369–393. [PubMed: 19768415]

8. Bramson J, Dayball K, Evelegh C, Wan YH, Page D, Smith A. Enabling topical immunization via microporation: a novel method for pain-free and needle-free delivery of adenovirus-based vaccines. Gene Ther. 2003; 10(3):251–260. [PubMed: 12571633]

9. Yuzhakov V. Skin microporation with PassPort(TM) system for continuous transdermal delivery of proteins. AAPS. 2005; 7(S1)

10. Sintov AC, Krymberk I, Daniel D, Hannan T, Sohn Z, Levin G. Radiofrequency-driven skin microchanneling as a new way for electrically assisted transdermal delivery of hydrophilic drugs. J Control Release. 2003; 89(2):311–320. [PubMed: 12711453]

11. Levin G, Gershonowitz A, Sacks H, Stern M, Sherman A, Rudaev S, Zivin I, Phillip M. Transdermal delivery of human growth hormone through RF-microchannels. Pharm Res. 2005; 22(4):550–555. [PubMed: 15846462]

12. Shapiro H, Harris L, Hetzel FW, Bar-Or D. Laser assisted delivery of topical anesthesia for intramuscular needle insertion in adults. Laser Surg Med. 2002; 31(4):252–256.

13. Bachhav YG, Summer S, Heinrich A, Bragagna T, Bohler C, Kalia YN. Effect of controlled laser microporation on drug transport kinetics into and across the skin. J Control Release. 2010; 146(1): 31–36. [PubMed: 20678988]

14. Park JH, Lee JW, Kim YC, Prausnitz MR. The effect of heat on skin permeability. Int J Pharma. 2008; 359(1–2):94–103.

15. Cohen ML. Measurement of thermal-properties of human-skin - review. J Invest Derm. 1977; 69(3):333–338. [PubMed: 894075]

16. Incropera, FP.; Dewitt, DP.; Bergman, TL.; Lavine, AS. Fundamentals of heat and mass transfer. John Wiley & Sons, Inc; Hoboken NJ: 2007.

17. Eppstein, JA.; Hatch, MR.; Yang, D. Microporation of human skin for drug delivery and monitoring applicaions. USA Patent. 2000.

18. English, BA.; Gadiraju, P.; Rinehart, CS.; Glezer, A.; Allen, MG. Gas generator actuator arrays for flight control of spinning body projectiles. 19th IEEE International Conference on MicroElectro Mechanical Systems (MEMS); Istanbul, Turkey. 2006.

19. Felder, RM.; Rousseau, RW. Elementary principles of chemical processes. John Wiley; New York: 2000. p. 637

20. Lee RC, Zhang DJ, Hannig J. Biophysical injury mechanisms in electrical shock trauma. Annu Rev Biomed Eng. 2000; 2:477–509. [PubMed: 11701521]

21. Defrin R, Ohry A, Blumen N, Urca G. Sensory determinants of thermal pain. Brain. 2002; 125:501–510. [PubMed: 11872608]

22. Fore J. The epidermal skin barrier: implications for the wound care practitioner, Part I. Advances in skin and wound care. 2004; 17(8):417–425. [PubMed: 15492677]

23. Carlson J. The Kodak one-time-use flash camera. Physics Teacher. 2004; 42(6):375–376.

24. Kalia YN, Bachhav YG, Bragagna T, Böhler C. P.L.E.A.S.E.® (Painless Laser Epidermal System). A new laser microporation technology. Drug Delivery Technology. 2008; 8:26–31.

25. Abbey, Norwood. Executive Informational Overview. Crystal Research Associates; New York: 2004. http://www.crystalra.com/pdf/Norwood_Abbey_EIO_12-15-04.pdf

26. Badkar AV, Smith AM, Eppstein JA, Banga AK. Transdermal delivery of interferon alpha-2B using microporation and iontophoresis in hairless rats. Pharma Res. 2007; 24(7):1389–1395.

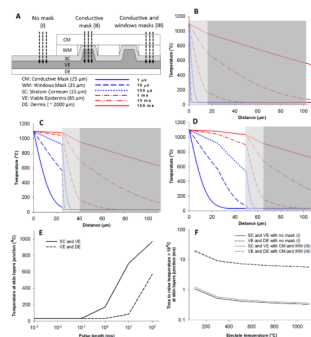27. Poling, BE.; Prausnitz, JM.; O'Connell, JP. The properties of gases and liquids. McGraw-Hill; New York: 2001.

Figure 1.
Simulation of the temperature profile across skin heated on its surface to 1100 °C for 1 μs to 100 ms. (A) Schematic diagram showing skin heating conditions. In (I), heat is directly applied to the skin. In (II), heat is applied to a conductive mask that is in direct contact with the skin on its underside. In (III), heat is applied to a conductive mask, below which is the solid portion of a windows mask, with skin on its underside. Below the schematic, abbreviations are defined and a legend for the graphs is provided as well. In the graphs, temperature profiles are shown as a function of depth into the skin, where the white region represents the mask, the light grey region represents the stratum corneum and the dark grey region represents the viable epidermis. Heat is applied (B) directly to the skin (case I) (C) through a conductive mask (case II), and (D) through a conductive and a windows mask (case III). Based on simulated temperature profiles shown for heating the skin surface directly to 1100 °C (case I), (D) the temperature at the stratum corneum-viable epidermis junction and at the viable epidermis-dermis junctions is shown as a function of time of heating. (E) The time required to increase skin temperature by 10 °C (i.e., from 32 °C to 42 °C) at the stratum corneum-viable epidermis junction and at the viable epidermis-dermis junction is shown as a function of ejectate temperature (i.e., skin surface temperature in case I).
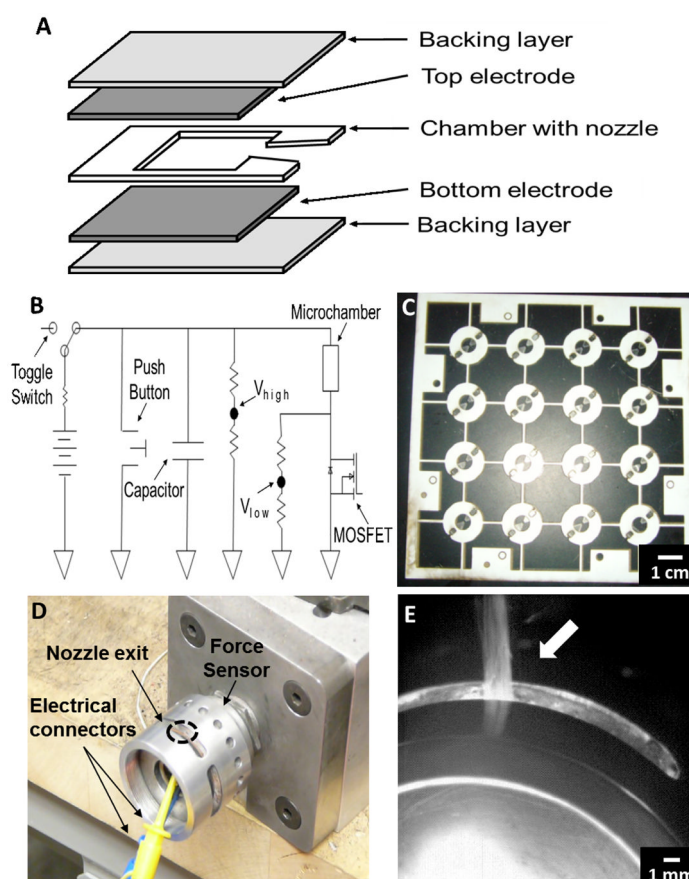
Figure 2.
Microsecond skin ablation system design. (A) Schematic diagram shows the five layers forming the microchamber. (B) Diagram of the electrical circuit used to generate an electrical discharge in the microchamber. (C) A set of 16 circular devices, each containing two microchambers (shown at the 1 o'clock and 7 o'clock positions) prepared by laser cutting the five layers shown in part (A) and laminating them together. (D) Photographic image of a microchamber device mounted in a force sensor. The microchamber nozzle exit is shown, as well as the electrical connectors to the power circuit. (E) Magnified view of the ejectate emitted from the microchamber obtained from a frame from a video collected at 100,000 frames per second.
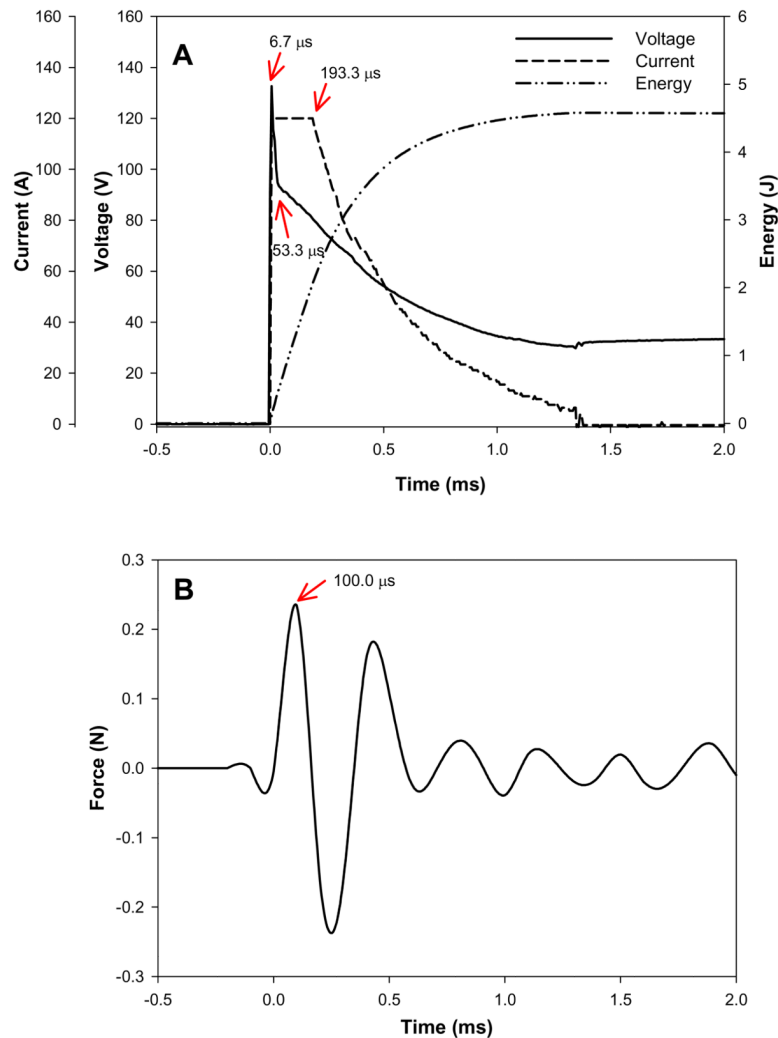
Figure 3.
Electrical and mechanical characteristics of microsecond thermal ablation system. (A) Voltage across the microchamber, current through the microchamber and cumulative energy release in the microchamber during an electrical discharge. The voltage peaked at 6.7 μs and then exhibited a biphasic decay until 1.3 ms, when the circuit was turned off. The current initially saturated with the MOSFET on and then decayed due to residual electrical pathways after electrical discharge in the microchamber. The cumulative energy increased and then plateaued at a value of 4.6 J. (B) Force measured by the force sensor during an electrical discharge. The force peaked at 100 μs and then oscillated down. The time and magnitude of the peak force is directly related to the force generated by the electrical discharge in the microchamber, whereas the subsequent oscillation is largely an artifact of the sensor.
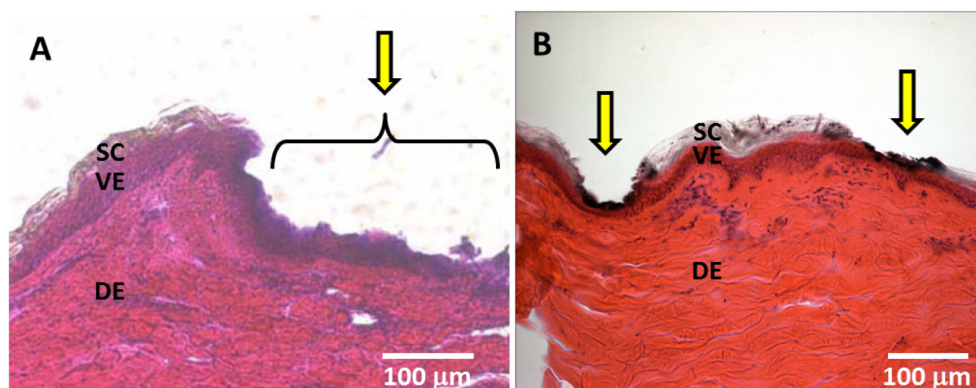
Figure 4.
Histological images of pig cadaver skin after microsecond thermal ablation (A) with no mask (Group 1 in Table 2) and (B) with a windows mask (Group 2 in Table 2). SC, VE, and DE represent stratum corneum, viable epidermis, and dermis, respectively. Arrows represent sites of thermal ablation. Skin stained with H&E.
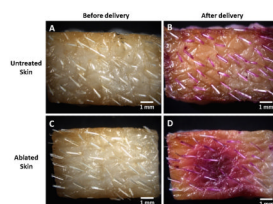
Figure 5.
Images of pig cadaver skin viewed *en face* after microsecond thermal ablation with a conductive mask (Group 3 in Table 2). Untreated skin is shown (A) before and (B) after topical delivery of sulforhodamine. Although the hairs are stained, there is essentially no staining of the skin. Ablated skin is shown (B) before and (D) after topical delivery of sulforhodamine. Sulforhodamine was applied to the skin surface for 12 h and then washed off before imaging. Dark staining of the skin with sulforhodamine indicates a breach of the skin barrier.
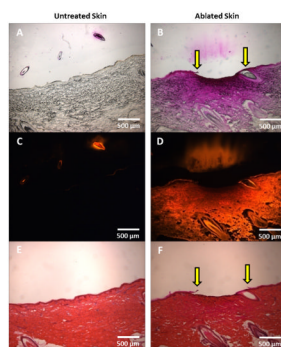
Figure 6.
Histological images of pig cadaver skin after ablation with a conductive mask (Group 3 in Table 2). Untreated skin (A, C, E) and ablated skin (B, D, F) are shown by brightfield imaging (A, B), fluorescence imaging (C, D), and again by brightfield imaging after H&E staining (E, F). Arrows indicate the edges of the ablated regions. Staining in images (A) through (D) indicate presence of sulforhodamine, which was applied to the skin surface for 12 h and then washed off before imaging.
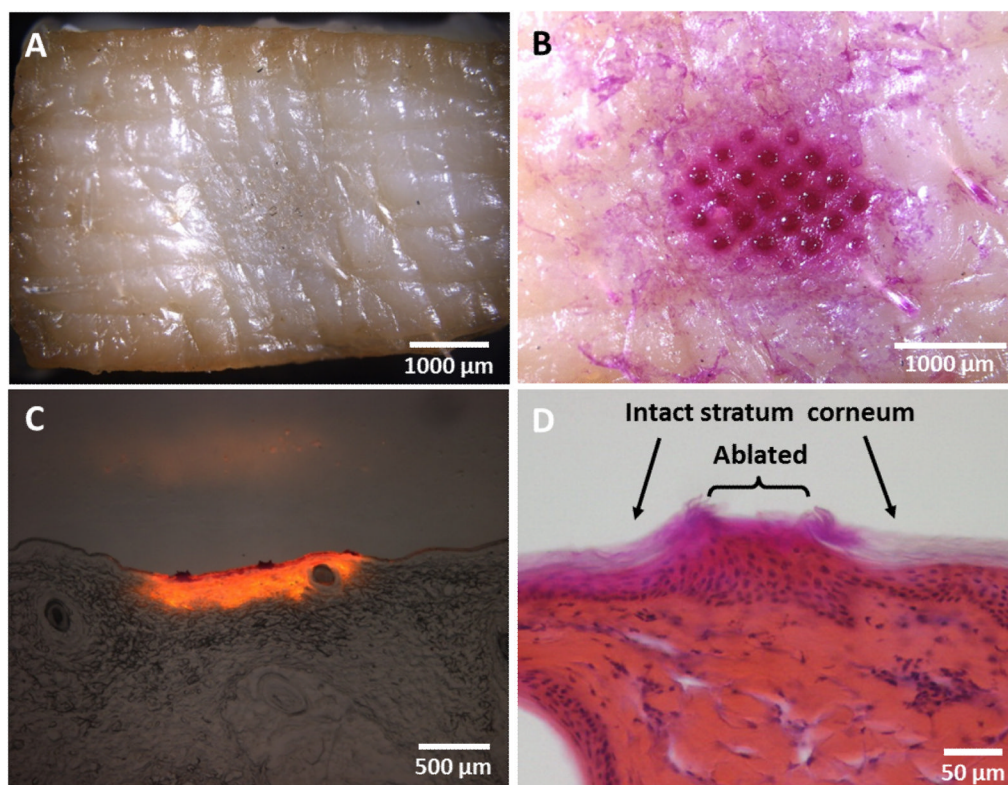
Figure 7.
Images of pig cadaver skin after ablation with a windows and conductive mask (Group 4 in Table 2). *En face* view of skin (A) after ablation and (B) after 30 min delivery of sulforhodamine to ablated skin. The array of darkly stained spots on the skin corresponds to the holes in the windows mask. (C) Histological image shown by a combination of brightfield and fluorescence optics after 30 min delivery of sulforhodamine to ablated skin. The dark spots on the skin surface correspond to sites of ablation through the windows mask and the brightly colored tissue below demonstrates delivery into the skin. (D) Histological images of ablated skin after H&E staining showing the site of ablation through one hole of the windows mask.
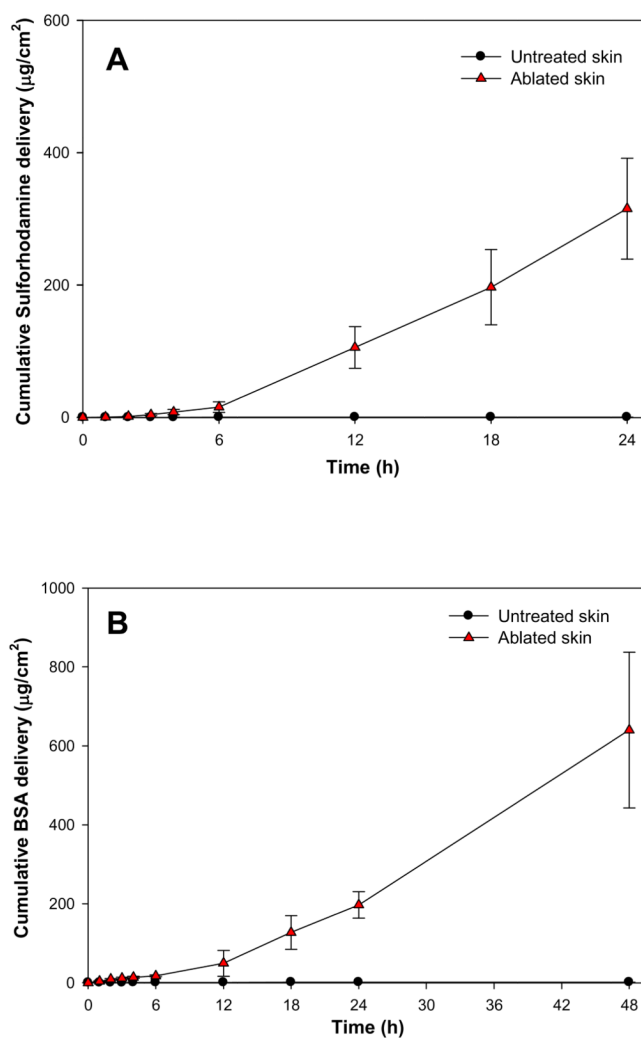
Figure 8.
Cumulative delivery of (A) sulforhodamine (558 Da) and (B) Texas Red-labeled bovine serum albumin (BSA; 66 kDa) across human cadaver skin after ablation with windows and conductive masks (Group 4 in Table 2). Permeation across ablated skin exhibited a lag followed by steady state delivery. Data represent the average ± standard deviation of = 5 replicate experiments.
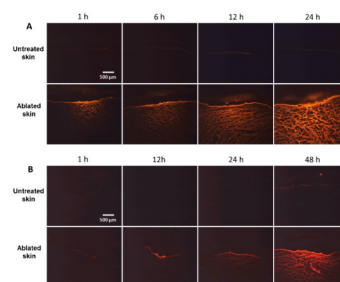
Figure 9.
Histological images of human cadaver skin after ablation with windows and conductive masks (Group 4 in Table 2) and delivery of (A) sulforhodamine and (B) BSA as a function of time and viewed by fluorescence microscopy. There was little penetration into untreated skin. In contrast, both molecules diffused deep into the ablated skin.

Table 1

Material property data used for modeling heat penetration into skin

Material	Thickness (μm)	Thermal conductivity (W/m·K)	Heat Capacity (J/kg·K)	Density (kg/m³)
Tungsten conductive mask	25	174	132	19300
Titanium windows mask	25	21.9	522	4500
Stratum corneum (SC)	15	0.123	1880	1280
Viable epidermis (VE)	85	0.42	3350	1090

Table 2

Schematic description of microsecond thermal ablation using four different mask arrangements.
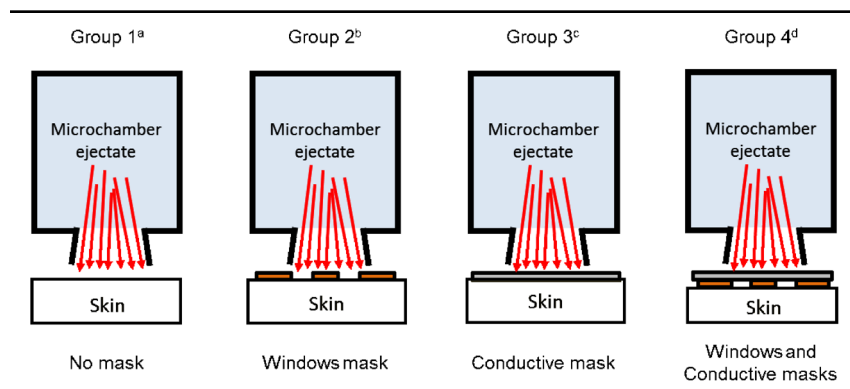
[a]Group 1 represents direct exposure of skin to thermal ablation with no mask.

[b]Group 2 represents thermal ablation with a windows mask to limit the skin surface area exposed to ablation.

[c]Group 3 represents thermal ablation with a conductive mask to prevent mechanical interaction between the ejectate and the skin, but still allow good heat transfer.

[d]Group 4 represents thermal ablation with a windows mask and a conductive mask to achieve the properties of both masks.